Strojniški vestnik - Journal of Mechanical Engineering 56(2010)1, 23-30
UDC 621.37
Paper received: 24.04.2009
Paper accepted: 23.10.2010

The Influence of Surface Topology on the Accuracy of Laser Triangulation Scanning Results

Nikola Vukašinović - Marjan Korošec - Jože Duhovnik
University of Ljubljana, Faculty of Mechanical Engineering, Slovenia

This paper discusses the influence of surface topology on the accuracy of laser triangulation scanning results. Scanning distance and scanning angle of impact laser beam was found to be the most crucial interaction between the surface topology and scanning process. Therefore, we focused these two parameters while other parameters like microstructure, colour of surface, optical settings remained fixed. Despite of random nature of freeform surfaces, the measurements were systematic, according to the principles of the design of experiment (DOE) adjusting angle and distance in the whole scanning range. Based on the results of this research and prior estimation of surface complexity, an implication or working area range prediction, as well as the determination of optimal set of influence parameters inside this particular working area can be done.
©2010 Journal of Mechanical Engineering. All rights reserved.
Keywords: laser measurer, surface topology, design of experiment (DOE), reverse engineering, laser scanning, laser triangulation

0 INTRODUCTION

To understand the complexity of laser triangulation scanning process we have to understand its working principles first. A laser scanner is a well known non-contact measuring and scanning device, widely applied in reverse engineering process used for acquisition of surface forms of 3D objects as well as in other fields of science, especially in medicine [1] to [3]. Their main components are illuminant and a sensor, which is usually CCD camera. The illuminant can be either coherent or incoherent. However, coherent illuminants such as lasers offer several distinct advantages over incoherent light sources [4]. The illuminant projects (usually) a light stripe on the surface of interest, while this projection is captured by the CCD sensor. Using a geometric triangulation method, a position of the illuminated spot according to the scanning coordinate system can be calculated, knowing the angles, and the baseline distance *d* between an illuminant and the picture of that spot on the sensor (Fig. 1), [5] and [6].

Despite of the simplicity of its working principle, there are numbers of parameters with complex interaction and evident influence on acquisition results. The main purpose of this work is, therefore, to clarify a part of this complexity and to give deeper sight into the importance of surface-scanner geometry for acquisition results.

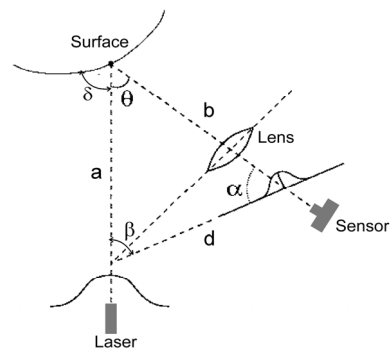

Fig. 1. *Geometric conditions to calculate a position of a point from a surface using triangulation principles [4]*

1 EXPERIMENTAL EQUIPMENT

The 3D noncontact measurement system consists of three-axis milling machine from the Flexmatic company, a Zephyr KZ-50 laser triangulation measuring sensor from the Kreon company, multifunction interface cards PCL-711, PCL-726, PCL-833 form the Systro company, and a personal computer for the coordination of the equipment. The layout of this 3D measuring system is shown in Fig. 2.

The X, Y, Z-measuring table is driven by AC servo motors. The encoder for each AC servo motor has a resolution of 2000 pulses per revolution.

*Corr. Author's Address: University of Ljubljana, Faculty of Mechanical Engineering, Aškerčeva 6, SI-1000 Ljubljana, nikola.vukasinovic@fs.uni-lj.si

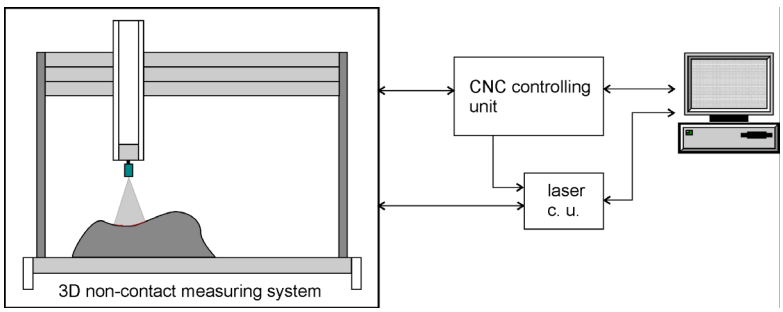

Fig. 2. *Measuring chain for laser triangulation scanning with CNC platform.*

Drivers for the AC servo motors are of the voltage control type. Multifunction interface cards, which include three channel encoders and counters, were used to read in the displacement data of each axis. The table was controlled by PC controller. The accuracy of the measuring table is 0.01 mm for each axis. The interface card PCL-711 has a 12 bit A/D channel to read in the laser displacement data. The resolution of the laser sensor is 0.005 mm, and repeatability is 0.006 mm. Hence, the two sigma accuracy of this measuring system is 0.04 mm. The system is controlled by PC that is used to handle all the I/O data from the controller. For the surface data acquisition Kreon hardware and Polygonia software are used. The signal achieved through RS232 serial link from the machine encoders and the signal from the laser sensor unit are simultaneously collected and merged to get the proper information about the surface geometry [7] to [10].

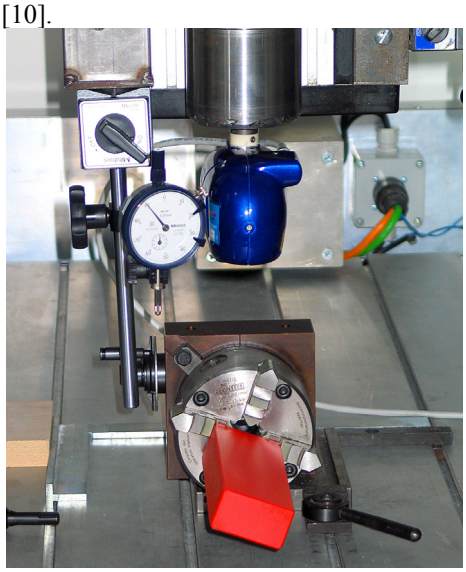

Fig. 3. *Scanning object fixed in a rotary head*

Coloured prismatic plate dimensions 150 × 50 × 30 mm, made of stone and polished (in order to get a smooth surface) was used to investigate the angle-distance standard deviation dependency (Fig. 3). The plate was fixed in a rotary head, which was rotated from 0 to 75 degrees, following 5 degrees increment, and randomised according to DOE principles [11] to avoid any unexpected machine drift. After getting point clouds captured, the standard deviation was calculated according to the ideally flat plane fitted through the point cloud using MatLab software. This procedure was repeated at different scan distances, from 60 to 120 mm, following 10 mm increment for all of the measured angles.

2 INFLUENCE OF SURFACE PROPERTIES

Before starting with the research work on the influence of the scanning angle and distance we have to briefly analyse other factors and parameters which exert influence on the accuracy of captured data. Since most of the optical parameters, which can be adjusted during the acquisition process were already widely analysed by Korošec et al. [12], we focus in this section mainly on the influence of surface colour.

Laser triangulation scanner uses a narrow spectrum of red light source to create a reflection stripe on the scanned surface to capture topology information. Therefore, we suspected that surface colour has a great influence on scanning results. So, it was necessary to research the reflection spectra of different surface colours. We investigated three different colours, i.e. red, green and blue, evenly distributed over the spectrum of visible wavelength and compared it with the referential white light. The spectrum of the sensor's light sources was also determined in the

same way. For that purpose, an electronic optical spectrometer Ocean Optics USB2000 was used.

Fig. 4 shows the results of spectral analysis. Different data sets were normalised to the same intensity level to achieve the possibility to compare the results. The black curve (1) shows the reflection of white light from the white surface and is used as the reference for other surface colours. The red (2), green (3) and blue (4) curves present spectra of white light reflected from three different coloured surfaces: red, green and blue. The dashed purple curve (5) represents the spectrum of sensor light reflected from the white surface. The first, lower but wider peak centred at 500 nm is caused by the green light diode, which helps positioning the scanner to the proper distance to the scanning object. The other, higher and narrower peak at 675 nm is the spectral response of the laser light source. This wavelength with ±10 nm threshold is also the working area of laser triangulation scanner. From the Fig. (4) it can be then seen, that in this area the best reflection provides white (100%) or red (87%) coloured surface, while green (23%) and blue (7%) surface provide much lower reflection. The red surface was chosen rather than the white since it reflects only the spectral part of red light between 600 and 700 nm while absorbing the energy of most of the other spectral field.

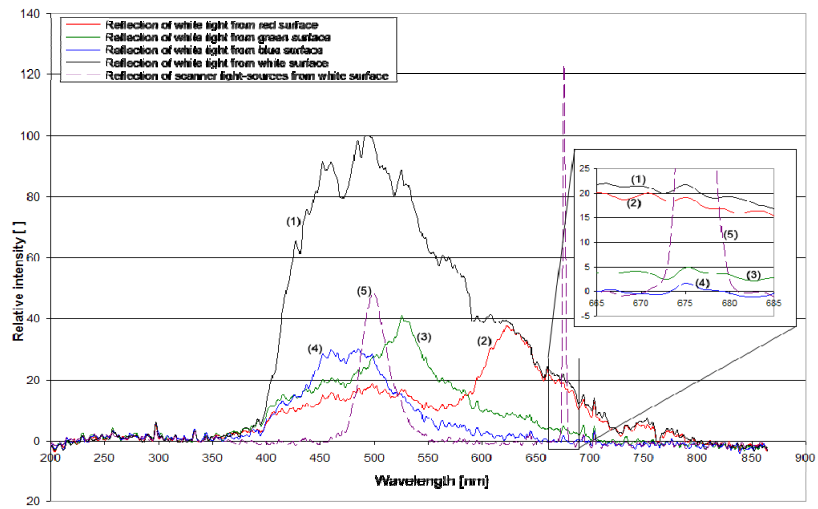

Fig. 4. *The spectrum of white light reflecting from different coloured surfaces and the reflection of sensor light sources from white surface*

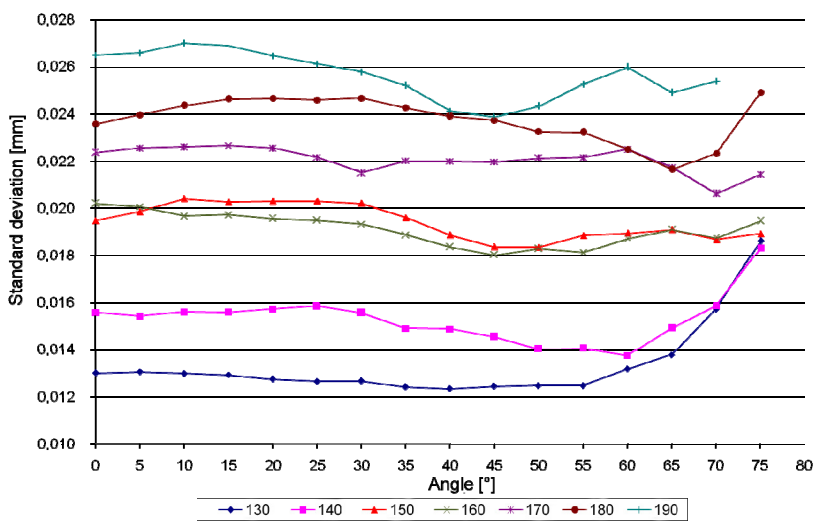

Fig. 5. *Standard deviation in YZ axes versus angle at different distances*

Table 1. *Standard deviation results at different angle-distance relations*

	Standard deviation YZ [mm]						
	Sensor-Surface distance [mm]						
Angle [deg]	70	80	90	100	110	120	130
0	0.0126	0.0156	0.0195	0.0202	0.0224	0.0236	0.0265
5	0.0126	0.0155	0.0199	0.0201	0.0226	0.0240	0.0266
10	0.0126	0.0156	0.0204	0.0197	0.0226	0.0244	0.0270
15	0.0125	0.0156	0.0203	0.0197	0.0227	0.0246	0.0269
20	0.0123	0.0158	0.0203	0.0196	0.0226	0.0247	0.0265
25	0.0121	0.0159	0.0203	0.0195	0.0222	0.0246	0.0261
30	0.0121	0.0156	0.0202	0.0193	0.0215	0.0247	0.0257
35	0.0118	0.0149	0.0196	0.0189	0.0220	0.0243	0.0251
40	0.0117	0.0149	0.0189	0.0184	0.0220	0.0239	0.0239
45	0.0117	0.0146	0.0184	0.0180	0.0218	0.0237	0.0238
50	0.0117	0.0140	0.0184	0.0183	0.0221	0.0233	0.0243
55	0.0116	0.0141	0.0189	0.0180	0.0221	0.0232	0.0253
60	0.0123	0.0138	0.0188	0.0186	0.0224	0.0225	0.0258
65	0.0128	0.0149	0.0191	0.0187	0.0217	0.0215	0.0246
70	0.0128	0.0149	0.0191	0.0187	0.0217	0.0215	0.0246
75	0.0173	0.0184	0.0189	0.0195	0.0217	0.0250	0.0249

angle. The observed size of the area element is

Table 2. *ANOVA results of chosen cubic design model*

Source	Sum of squares	*df*	Mean square	*F*-value	*p*-value *Prob > F*	
Model	2.003E-003	9	2.225E-004	243.38	< 0.0001	significant
A-distance	1.941E-004	1	1.941E-004	212.30	< 0.0001	
B-angle	2.822E-005	1	2.822E-005	30.87	< 0.0001	
AB	1.459E-005	1	1.459E-005	15.96	0.0001	
A^2	1.893E-005	1	1.893E-005	20.71	< 0.0001	
B^2	1.432E-005	1	1.432E-005	15.66	0.0001	
A^2B	1.905E-006	1	1.905E-006	2.08	0.1519	
AB^2	5.642E-006	1	5.642E-006	6.17	0.0146	
A^3	4.815E-006	1	4.815E-006	5.27	0.0238	
B^3	1.972E-005	1	1.972E-005	21.57	< 0.0001	
Residual	9.325E-005	102	9.142E-007			
Cor Total	2.096E-003	111				
Std. Dev.	9.561E-004		R-Squared	0.9555		
Mean	0.020		Adj R-Squared	0.9516		
C.V. [%]	4.87		Pred R-Squared	0.9465		
PRESS	1.121E-004		Adeq Precision	51.637		

To achieve the best possible scanning results, colours with diffuse reflection were used, and therefore, the Lambert model of reflected light distribution was supposed. Lambert reflection model says that the surface luminance is the same, regardless of the view angle. However, the reflected power from an area element is reduced by the cosine of the reflection also reduced by that same amount. This phenomenon can be observed by changing the surface lean angle according to the machine table plane and varying the distance between the surface and sensor [13].

The results, which were obtained according to the procedure described in previous sections, are numerically presented in Table 1 and

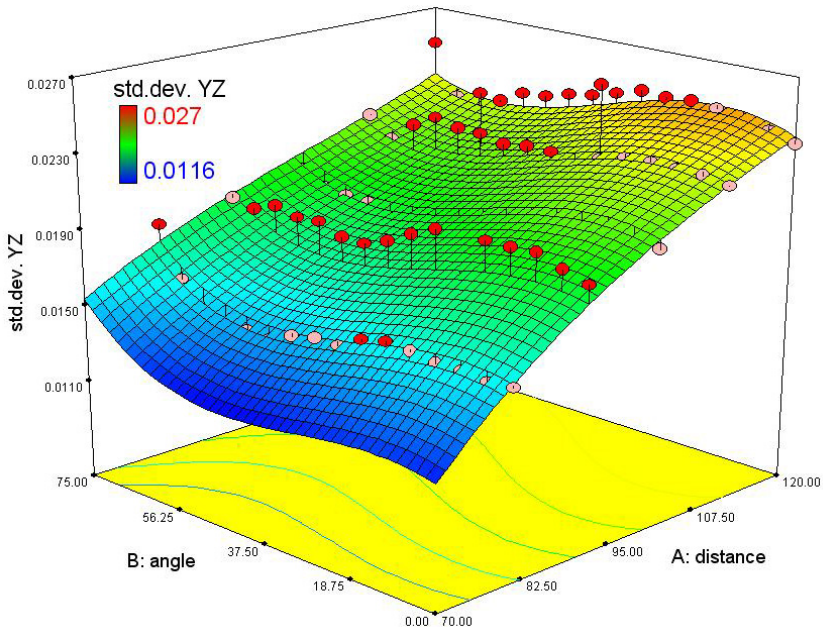

Fig. 6. *Factorial response surface plot of angle-distance relations*

graphically in Fig. 5. The graph shows that the standard deviation rate is slightly decreasing towards 55 degrees and then progressively increasing. It is also smaller with a smaller sensor-surface distance. It is, therefore, obvious, that the desired area of operation is at small distances and surface lean angles below 55 degrees. Since the standard deviation in X axis was constant through all of the measured results, it was excluded from the calculation. These results will be further used in the next section for setting the design model.

3 ANOVA ANALYSIS AND BUILDING OF MATHEMATICAL MODEL

The general full factorial design consisted of 112 experimental runs (with two replicas), taken at 7 levels of distance and 16 levels of lean angle. This design of experiment was used for the Anova analysis and for building up a suitable mathematical-design model.

The Anova results for response surface cubic model according to experimental results from Fig. 6 are presented in Table 2.

The model *F*-value of 243.38 implies the model is significant. There is only a 0.01% chance that a "Model *F*-Value" this large could occur due to the noise. Values of "*Prob* > *F*" smaller than 0.05 indicate model terms are significant. In this case A, B, AB, A^2, B^2, AB^2, A^3, B^3 are significant model terms. Values greater than 0.1 indicate the model terms not to be significant. The "Pred R-Squared" of 0.9465 is in reasonable agreement with the "Adj R-Squared" of 0.9516. "Adeq Precision" measures the signal to noise ratio. A ratio greater than 4 is desirable [14]. Ratio of 51.637 indicates an adequate signal. So this model can be used to navigate the design space.

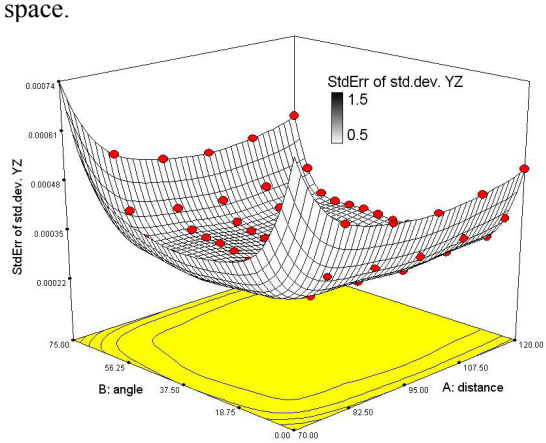

Fig. 7. *Standard error plot of angle-distance design area*

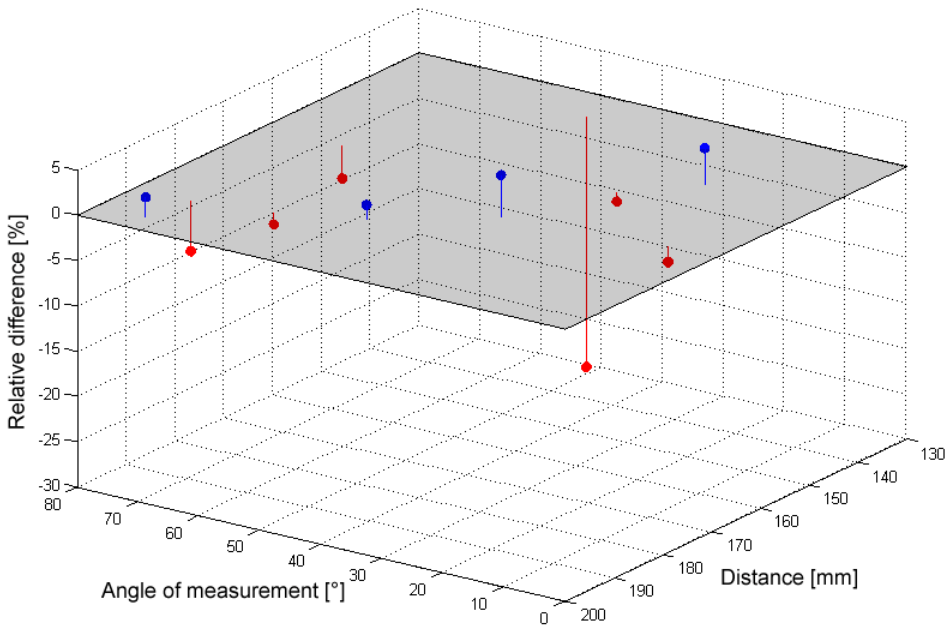

Fig. 8. *Relative difference between measured and calculated results for 10 randomly selected angle-distance combinations*

Further, an equation model of standard deviation in YZ axes in terms of coded factors was created (Eq. (1)):

$$\begin{aligned}\text{std.dev. YZ} = {} & \\ & +0.018 \\ & +6.996E-003 \times A \\ & -2.270E-003 \times B \\ & -1.462E-003 \times A \times B \\ & -1.925E-003 \times A^2 \\ & +1.199E-003 \times B^2 \\ & +8.161E-004 \times A^2 \times B \\ & -1.176E-003 \times A \times B2 \\ & +8.764E-004 \times A^3 \\ & +2.563E-003 \times B^3.\end{aligned} \quad (1)$$

The equation can be transformed to use actual factors (Eq. (2)), consisting angle and Sensor-Surface distance:

$$\begin{aligned}\text{std.dev. YZ} = {} & \\ & -0.051650 \\ & +1.57980E-003 \times \text{distance} \\ & +2.05338E-004 \times \text{angle} \\ & -3.56248E-006 \times \text{distance} \times \text{angle} \\ & -1.18102E-005 \times \text{distance}^2 \\ & -2.10757E-006 \times \text{angle}^2 \\ & +2.41814E-008 \times \text{distance}^2 \times \text{angle} \\ & -2.78682E-008 \times \text{distance} \times \text{angle}^2 \\ & +3.24606E-008 \times \text{distance}^3 \\ & +4.86063E-008 \times \text{angle}^3.\end{aligned} \quad (2)$$

In Fig. 7a well predicted pocket region is noticeable, where standard deviation predictions should be very reliable. This is the inner square, extended from 16 to 60° and from 82 to 110 mm distances. At this point, it is necessary to emphasize that a good prediction area does not directly coincide with the area of smallest standard deviation, which can be predicted from the Fig. 6.

4 EXPERIMENTAL VERIFICATION OF DESIGN MODEL

The accuracy of the equation model was tested with ten randomly chosen distance-angle level combinations. Testing was done by comparing the calculated standard deviation values for chosen combinations with the values which were measured as depicted in previous sections. The combinations, measured standard deviation value and the predicted standard deviation value are collected in Table 3. Fig. 8 graphically shows the results of comparison. It can be seen that the difference does not exceed 5%, except at one border point where bigger divergence was also expected (compared with Fig. 7).

To evaluate the relative performance of the developed design model in Eq. (2), the mean absolute percentage deviation (MAPD) between measured and calculated results was used:

$$MAPD = \frac{1}{m}\sum_{k=1}^{m}\left|\frac{\left(\hat{Y}_k - Y_k\right)}{Y_k}\right| = 0.0536 \qquad (3)$$

where $\hat{Y}_k$ is calculated output and Y_k is the corresponding measured output [15]. The MAPD value of 5.36% is acceptable, and indicates that the calculated values by the presented mathematical design model are in a satisfactory agreement with the measured values according to the 5.36% error.

Table 3. *Verification test of equation model with ten randomly chosen distance-angle level combinations*

angle	dist.	pred. std. dev.	meas. std. dev.
8	109	0.0226	0.0222
18	89	0.0188	0.0196
26	97	0.0198	0.0196
33	112	0.0227	0.0238
47	77	0.0120	0.0094
47	122	0.0232	0.0236
59	126	0.0236	0.0233
67	102	0.0200	0.0193
71	128	0.0244	0.0231
72	136	0.0262	0.0268

5 CONCLUSION

The experiment was done to evaluate the influence of sensor-surface distance, surface lean angle and their interaction on the accuracy of scanning results. According to the results an equation model for error estimation was also developed. The results showed that these two parameters have an important influence on the accuracy of gathered information. The best results were achieved at small sensor-surface distances, while the angle has a slight decreasing influence on error all to 55 degrees where the line turns drastically upwards. Therefore, we would suggest the use of the smallest possible scanning distances and angles up to 55 degrees. The future goal is to investigate the influence of the surface curvature on the accuracy of results and to develop a method for estimating scanning errors for arbitrary freeform surface before the scanning process is done. In the next step, this would allow the optimisation of main scanning parameters to achieve the best possible results in a shorter period of time.

6 REFERENCES

[1] Bračun, D., Jezeršek, M., Diaci, J. Triangulation model taking into account light sheet curvature, *Measurement Science and Technology*, 2006, vol. 17, pp. 2191-2196.

[2] Vukašinović, N., Kolšek, T., Duhovnik, J. Case study - surface reconstruction from point clouds for prosthesis production, *Journal of eng. design.*, 2007, vol. 18, no. 5, p. 475-488.

[3] Jezeršek, M., Fležar, M., Možina, J. Laser Multiple Line Triangulation System for Real-time 3-D Monitoring of Chest Wall During Breathing, *Strojniški vestnik – Journal of Mechanical Engineering*, 2008, vol. 54, no. 7-8, p. 503-506.

[4] Curles, B.L. *New methods for surface reconstruction from range images,* Department of Electrical Engineering of Stanford University, 1997. Retrieved on 15. 3. 2009, from http://www-graphics.stanford.edu/papers/curless_thesis/

[5] Huang, S.J., Lin, C.C. A three-dimensional non-contact measuring system, IJAMT, 1997, vol. 13, p. 419-425.

[6] Shiou, F.J., Ali, Y.C. Development of a non-contact multiaxis reverse engineering measurement system for small complex objects. In: Publishing Journal of Physics, 2005, Conference Series 13, 7th International Symposium on Measurement Technology and Intelligent Instruments, p. 419-425.

[7] ISEL Automation KG ISEL Automation katalog, Mechanics und Electronics, Leibolzgraben, Technical report, 2004.

[8] Kreon Technologies, Polygonia Training, Technical report, 2005.

[9] Kreon Technologies, Polygonia, 3D digitalization system, Technical report, 2005.

[10] Kreon Technologies, Integration of the Kreon scanner on arms and 3 axis machines, Technical report, 2005.

[11] Mason, R.L., Gunst, R.F., Hess, J.L. *Statistical design and analysis of experiments with applications to engineering*

and science, Second edition, John Willey and Sons, Inc, 2003.

[12] Korošec, M., Duhovnik, J., Vukašinović, N. Process modeling of non-contact reverse engineering process. In: *Proceeding of the 7th WSEAS International Conference on Signal Processing, omputational Geometry and Artificial Vision ISCGAV'07*, Athens, Greece, 2007.

[13] Nassau, K. *The physics and chemistry of color*, (The fifteen causes of color). Second edition. John Willey and Sons, Inc, 2002.

[14] Montgomery, D.C. *Design and analysis of experiments*, Arizona State University, John Willey and Sons, Inc, 2001.

[15] Vapnik, V. *Statistical learning theory*, John Willey and Sons, Inc, 1998.